

Silica-Functionalized Nanolimes for the Conservation of Stone Heritage

Miguel Burgos-Ruiz,* Kerstin Elert, Encarnacion Ruiz-Agudo, Helmut Cölfen, and Carlos Rodriguez-Navarro

The relatively recent development of nanolimes (i.e., alcoholic dispersions of $\text{Ca}(\text{OH})_2$ nanoparticles) has paved the way for new approaches to the conservation of important art works. Despite their many benefits, nanolimes have shown limited reactivity, back-migration, poor penetration, and lack of proper bonding to silicate substrates. In this work a novel solvothermal synthesis process is presented by which extremely reactive nanostructured $\text{Ca}(\text{OH})_2$ particles are obtained using calcium ethoxide as the main precursor species. Moreover, it is demonstrated that this material can be easily functionalized with silica-gel derivatives under mild synthesis conditions, thereby preventing particle growth, increasing total specific surface area, enhancing reactivity, modifying colloidal behavior, and functioning as self-integrated coupling agents. Additionally, the formation of calcium silicate hydrate (CSH) nanoce-ment is promoted by the presence of water, resulting in optimal bonding when applied to silicate substrates, as evidenced by the higher reinforcement effect produced on treated Prague sandstone specimens as compared to those consolidated with nonfunctionalized commercial nanolime. The functionalization of nanolimes is not only a promising strategy for the design of optimized consolidation treatments for the cultural heritage, but may also have important implications for the development of advanced nanomaterials for building, environmental, or biomedical applications.

many menacing chemical, physical and biological alteration processes it faces, whether natural or anthropogenic in nature.^[1–8] Over the last two decades, nanotechnology has contributed to the development of promising solutions for the protection and conservation of cultural heritage, among several other applications. For this reason, nanolimes (i.e., calcium hydroxide nanoparticles) have been in the scope of both scientists and conservators, as they provide an effective solution to the shortcomings of conventional consolidation treatments for porous substrates (e.g., stone, mortars, ceramics, and wall paintings), specifically the usually poor compatibility, limited durability, and effectiveness of synthetic polymers and alkoxysilanes.^[9–12]

Nanolimes consolidate a porous substrate via reaction with atmospheric CO_2 , forming CaCO_3 cement. This carbonation reaction also occurs during application of limewater (i.e., a saturated $\text{Ca}(\text{OH})_2$ aqueous solution), used as a traditional consolidant for centuries.^[13,14] However, the low solubility of portlandite ($\text{Ca}(\text{OH})_2$)


limits its efficacy,^[15] as the use of large volumes of limewater is required to achieve a reasonable degree of consolidation. This is especially prohibitive in the case of water-sensitive substrates.^[16,17] To overcome the limitations of limewater, alcoholic calcium hydroxide suspensions were introduced, containing larger amounts of consolidant and displaying good colloidal stability, low surface tension, and an acceptable penetration capacity in porous substrates.^[18,19] Their dispersion in aliphatic alcohols eliminates any possible water-related damage (e.g., salt mobilization, or freeze damage). Aiming at producing nano-sized, highly reactive $\text{Ca}(\text{OH})_2$ crystals, Baglioni's group developed a homogeneous synthesis method to produce particles 50–500 nm in size (with a specific surface area, SSA, of up to $\approx 35 \text{ m}^2 \text{ g}^{-1}$), which are dispersed in ethanol or isopropanol and commercialized under the tradename Nanorestore.^[20–22] However, this method involved tedious purification processes using water, which lead to particle coarsening.^[23] This is an important drawback, because particles with larger sizes generally have lower SSA, reactivity and penetrability in a porous substrate. In 2005, Ziegenbalg et al. patented a solvothermal procedure for the synthesis of nanolimes (though, conditions of synthesis

1. Introduction

The survival of our architectural and sculptural heritage greatly depends on the design of effective strategies to counteract the

M. Burgos-Ruiz, K. Elert, E. Ruiz-Agudo, C. Rodriguez-Navarro
Department of Mineralogy and Petrology
University of Granada
Av. Fuentenuueva s/n, Granada 18002, Spain
E-mail: miguelburgos95@ugr.es

H. Cölfen
Physical Chemistry
Department of Chemistry
University of Konstanz
Universitätsstraße 10, D78457 Konstanz, Germany

 The ORCID identification number(s) for the author(s) of this article can be found under <https://doi.org/10.1002/smll.202300596>.

© 2023 The Authors. Small published by Wiley-VCH GmbH. This is an open access article under the terms of the Creative Commons Attribution License, which permits use, distribution and reproduction in any medium, provided the original work is properly cited.

DOI: 10.1002/smll.202300596

were not specified) whereby highly reactive particles 30–300 nm in size (SSA of up to $\approx 35\text{--}40\text{ m}^2\text{ g}^{-1}$) are obtained and commercialized as alcoholic dispersions under the trademark Calosil (Figure S1, Supporting Information).^[24] While in the case of carbonate substrates (e.g., limestone, plaster, and marble) an adequate consolidation upon application of these nanolimes is often reported, some drawbacks have been encountered: (a) limited reactivity after particle coarsening during synthesis and purification; (b) poor penetration in porous substrates associated with back-migration of the nanoparticles during solvent evaporation; and (c) lack of proper bonding between the newly formed CaCO_3 cement and silicate substrates (e.g., sandstone, tuff, granites, or ceramics).^[1,6,11,18]

The potential use of $\text{Ca}(\text{OH})_2$ nanoparticles to capture gaseous pollutants (e.g., CO_2 or SO_2) has also prompted research into different methods to produce calcium and magnesium hydroxide nanoparticles. Kirchgessner et al. patented a method for the synthesis of calcium hydroxide by slaking quicklime in the presence of calcium lignosulfonate. In this way, micrometric size portlandite aggregates with SSA of up to $40\text{ m}^2\text{ g}^{-1}$ were obtained for their use in SO_2 capture.^[25] More recently, the company Lhoist S.A. developed a high-yield industrial process for obtaining highly porous and reactive $\text{Ca}(\text{OH})_2$ particles by controlled hydration of calcium oxide using industrial hydrators and mill flash dryers.^[26] The disadvantage of this method lies in the poor control over the particle size and the formation of large oriented aggregates, which cannot be redispersed in alcohol.^[27] Also, the efficacy of this product is limited due to the formation of passivation layers that prevent complete reaction, making further purification steps necessary to reuse the unreacted material.^[28]

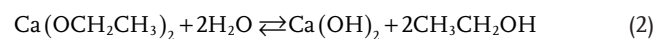
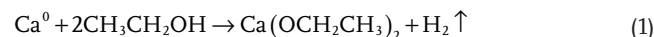
Here we report on a novel method to obtain silica-functionalized portlandite nanoparticles (Si-NL) showing well-developed (001) faces and plate-like morphology, minimal aggregation, and extremely high SSA, using a one-pot solvothermal synthesis procedure, originally developed by our group for the production of phase-pure bassanite ($\text{CaSO}_4 \cdot 0.5\text{H}_2\text{O}$) nanorods via hydrolysis of amorphous calcium ethoxide as the main intermediate species.^[29] This method solves several limitations of previous synthesis strategies, as it has a high yield, does not require the removal of residual salts or additives, and allows for a circular production as all solvents can be distilled and recycled. In addition, it enables the simultaneous functionalization of the portlandite nanoparticles with silica-gel derivatives that are able to generate nanocementitious CSH interfaces. These silica-functionalized nanolimes are very promising candidates not only for improved consolidation treatments in the field of heritage conservation, but also for other technical applications such as acid gas capture and storage, heterogeneous catalysis or the design of advanced building and biomedical materials.^[30–33]

2. Results and Discussion

2.1. Synthesis of Si-NL

Si-functionalized portlandite nanoparticles (Si-NL) were obtained following a modification of the in-house developed one-pot solvothermal procedure for the phase-selective

synthesis of bassanite nanorods.^[29] In this case, the reaction mechanism (Figure 1a) proceeds in two steps as follows:



In a typical synthesis run, during the first step (Equation 1), a white suspension of amorphous calcium ethoxide is obtained by the irreversible oxidation of 2 g of pure metallic calcium in 200 mL of absolute ethanol at 80 °C under reflux condensation conditions. Afterwards, calcium hydroxide nanoparticles precipitate by the controlled hydrolysis of calcium ethoxide (Equation 2) upon addition of 10 mL deionized water and 80 mL toluene, which locally increases the activity coefficient of water and speeds up the hydrolysis of calcium ethoxide. Finally, solvents are eliminated by rotary evaporation, yielding 3.5 g of Si-NL in the form of a white powder. It is important to mention that all these synthesis steps were initially performed using a glass reactor, from which SiO_2 leached under the synthesis pH and T conditions and partially transformed into silica-gel derivatives^[34,35] that deposited on the surface of $\text{Ca}(\text{OH})_2$ particles as a highly porous nanostructured silica/CSH coating.^[36] Further details on the materials used and synthesis route, as well as characterization methods and analytical techniques (see below) are presented in the Supporting Information.

2.2. Characterization of Si-NL

The X-ray diffraction (XRD) patterns of Si-NL show broad 00l and 0kl and narrow h00 Bragg peaks of portlandite ($P\bar{3}m_1$) indicating poorer crystallinity along the c-axis than along the a-axis (Figure 1b). This is consistent with Scherrer crystallite size measurements, yielding $D_{001} = 8\text{ nm}$ and $D_{100} = 28\text{ nm}$. These results indicate that the Si-NL powder is composed of extremely thin hexagonal plates of about ten to fifteen unit-cells (measured along the [001] direction), which is in good agreement with the results obtained by transmission electron microscopy (TEM, see below).

Fourier-transform infrared (FTIR) spectra of Si-NL (Figure 1d,e) showed an intense narrow band at 3642 cm^{-1} associated with O–H bonds (ν O–H) in calcium hydroxide, along with a band at 1650 cm^{-1} ascribed to the bending (δ O–H) of water, a broad band at 1440 cm^{-1} (ν_3 asym. CO_3) and a narrow band at 880 cm^{-1} (ν_2 asym. CO_3) corresponding to a small amount of amorphous calcium carbonate (ACC, formed during sample handling), consistent with the absence of calcite Bragg peaks in the Si-NL XRD pattern. Furthermore, traces of unreacted calcium ethoxide were identified as a band triplet of C–H bond stretch vibrations (ν C–H) at 2956, 2900, and 2800 cm^{-1} , along with a moderately intense C–O stretching doublet (ν C–O) in the fingerprint region at 1114 and 1058 cm^{-1} .^[37] The presence of trace amounts of silica derivatives was confirmed by a low intensity broad band ranging from 960 to 1040 cm^{-1} and a low intensity peak at 3692 cm^{-1} , respectively, corresponding to Si–O (ν Si–O) and SiO–H (ν SiO–H) bonds in the silica coatings (Figure 1d,e).^[38]

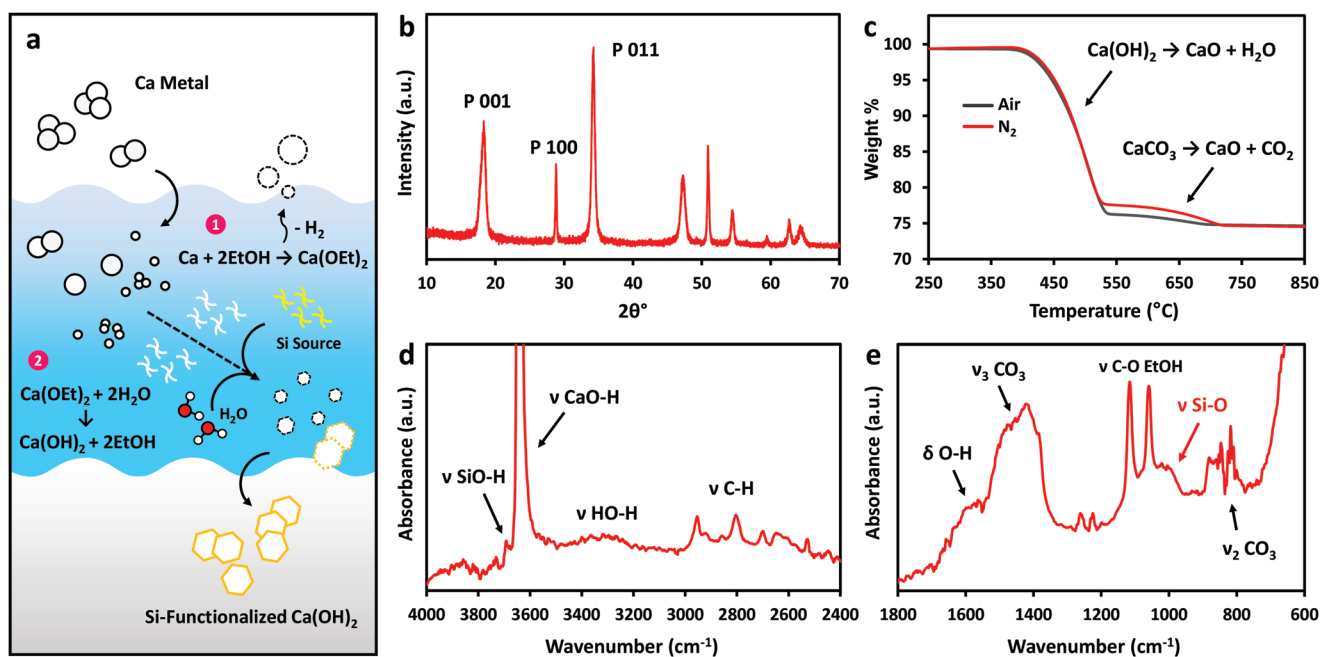


Figure 1. a) Synthesis schematic and characterization of Si-NL. b) Broad 00l and 0kl Bragg peaks in the XRD patterns confirm that Si-NL is composed of extremely thin portlandite plates. c) TGA in both air (black) and N₂ (red) allowed to determine that the yield % of the complete synthesis was >95%. d,e) The FTIR spectra revealed small amounts of unreacted calcium ethoxide (low-intensity sharp bands at 1114 and 1058 cm⁻¹) and silanol groups (broad Si–O stretching band at ≈1000 cm⁻¹ and weak SiO–H stretching peak at 3692 cm⁻¹), along with Ca(OH)₂ (sharp and intense O–H stretching band at 3642 cm⁻¹).

Thermogravimetry (TGA) curves obtained in both air and N₂ permitted the calculation of the amount of unreacted calcium ethoxide in the final product (Figure 1c). Under inert N₂ atmosphere conditions, a weight loss of 24.00 wt% from 450 to 600 °C, associated with the endothermic dehydroxylation of calcium hydroxide (Ca(OH)₂ → CaO + H₂O), and a small weight loss of 1.40 wt% from 600 to 800 °C, ascribed to the thermal decomposition of calcium carbonate (CaCO₃ → CaO + CO₂), could be observed. Under oxidizing conditions, in contrast, these endothermic processes resulted in mass losses of 22.80 and 2.70 wt% respectively, indicating that the combustion of calcium ethoxide and the spontaneous carbonation of the originated calcium oxide (Ca(OCH₂CH₃)₂ + 6O₂ → CaO + 4CO₂ + 5H₂O; CaO + CO₂ → CaCO₃) occurred simultaneously with the dehydroxylation of Ca(OH)₂.^[39] The difference between the amount of decomposed CaCO₃ indicates that the synthesized nanolime was minimally carbonated (2.40 wt%) and contained a small amount of unreacted calcium ethoxide (4.70 wt%). The remaining wt% corresponded to pure portlandite (92.87 wt%) and adsorbed water (0.03 wt%). Considering that ACC originates from sample manipulation, a yield higher than 95% can be assumed.

TEM analysis (Figure 2a; Figure S2, Supporting Information) revealed that Si-NL consisted of non-oriented aggregates (as shown by the angular spreading of the 110 reflections shown in the SAED pattern (Figure 2a, inset) made up of crystalline and relatively monodisperse thin plate-like portlandite nanoparticles. The measured particle equivalent diameter (along the *a* or *b* directions) ranged from 20 to 120 nm and their widths (measured along the *c* direction) ranged from 5

to 25 nm, dimensions that are significantly smaller than those of commercial nanolimes. Scanning TEM (STEM) energy dispersive X-ray spectrometry (EDX) elemental maps and spectra were decisive to prove that silica accumulated on the surface of the produced Ca(OH)₂ nanoparticles (Figure 2b,c; Figure S3, Supporting Information). Further analyses performed on carbonated Si-NL (Figure 2d–f) showed that the silica coatings remained on the surface of newly formed calcite particles after carbonation, suggesting the formation of calcium silicate hydrate (CSH) interfaces.

Solid-state NMR results provided additional qualitative information about the chemical nature of the silica nanostructures. The ²⁹Si NMR spectra of both carbonated and noncarbonated Si-NL (Figure 3a,b) showed a broad band of moderate intensity at δ(²⁹Si) ranging from –50 to –150 ppm, with a maximum at –108.1 ppm and a shoulder at –117.7 ppm corresponding to Q³ and Q⁴ –Si–O–Si– structures, respectively, typically ascribed to amorphous SiO₂ (i.e., silica-gel). Additionally, a low intensity peak at –71.8 ppm alongside a shoulder at –82.5 ppm and a maximum at –92.6 ppm could be ascribed to Q⁰, Q¹, and Q² structural units, respectively, corresponding to CSH species.^[40,41] Silanol and siloxane functional groups were also identified by the moderate intensity shoulder at –130.6 ppm and the low intensity peak at –146.2 ppm respectively. ¹H NMR spectra (Figure 3c) for both samples suggest that nanofilms initially contained small amounts of CSH, as revealed by the peak at +6.2 ppm (CSH (Si–)O–H bonds), which showed a significant increase in intensity after carbonation. This latter confirms that the concentration of CSH phases increases upon carbonation (see below).

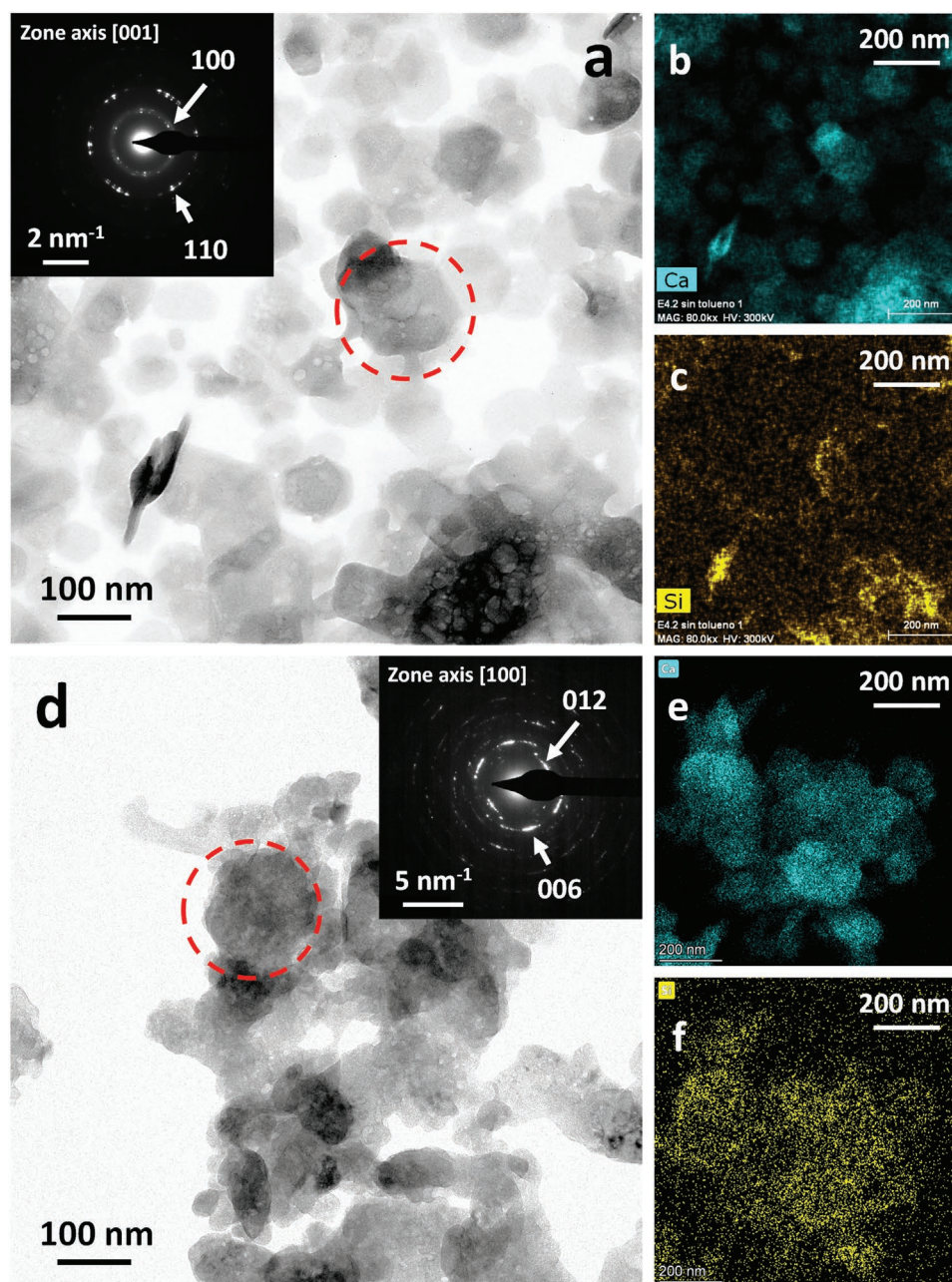


Figure 2. TEM photomicrographs of a) non carbonated and d) carbonated non-oriented Si-NL aggregates. c,f) The STEM-EDX elemental Si maps confirmed the presence of silica covering the nanoparticles. b,e) Elemental Ca maps are included for reference.

BET analysis of the N_2 sorption isotherms (Figure S4a, Supporting Information) shows that Si-NL has extremely high SSA values of up to $80 \text{ m}^2 \text{ g}^{-1}$, which are among the highest values reported for similar products in the literature. The increase in SSA as compared with commercial nanolimes could be explained by the overall decrease in particle size, as well as the high aspect ratio of the very thin, plate-like nanoparticles.^[42] Additionally, the presence of the highly porous silica coatings might account for 5–10% of the total SSA.^[42,43] Functionalized nanolime particles exhibited a Type II isotherm with a H3 hysteresis loop corresponding to non-microporous solids with slit-shaped pores, standard features of portlandite powders.^[18]

XRF analyses of Si-NL and the calcium ethoxide precursor synthesized in a glass reactor (Table S1, Supporting Information) revealed that both contained Si in low concentrations of 0.01 and 0.02 wt% (measured as SiO_2 wt%), respectively. This means that SiO_2 lixiviation from glassware occurred not only during the hydrolysis of calcium ethoxide, but also during its formation. Silica lixiviation is due to the high pH reached during synthesis (note that silica solubility increases exponentially at $\text{pH} > 9$).^[44] Because the $\text{Ca}(\text{OH})_2$ surfaces, and in particular the (001) faces (those with the highest development in the plate-like particles of Si-NL), are positively charged due to the presence of abundant $-\text{CaOH}_2^+$ surface species at alkaline pH

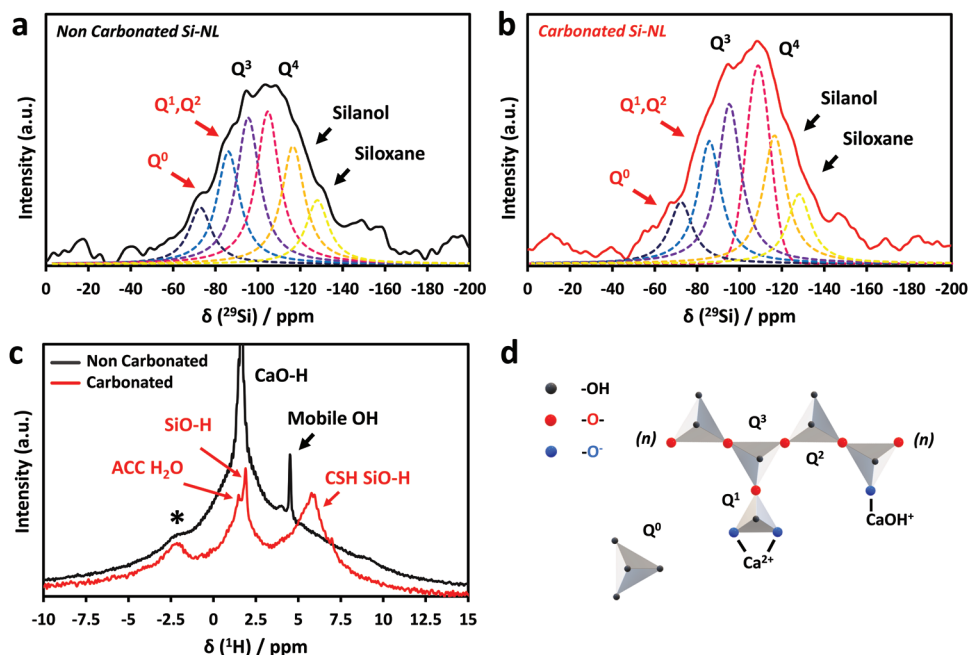


Figure 3. ^{29}Si solid state NMR spectra of a) non carbonated and b) carbonated Si-NL demonstrating the presence of CSH (including Q^0 – Q^2 structural groups), and other silica derivative species (Q^3 – Q^4) originating $\delta(^{29}\text{Si})$ chemical shifts between -50 and -150 ppm. Deconvolution ($R^2_a = 0.957$ and $R^2_b = 0.945$) allowed to distinguish between Q^0 to Q^4 units, silanol and siloxane structural groups. Chemical shift $\delta(^1\text{H})$ signals in the c) NMR spectra revealed that the composition of nanofilms evolved upon hydration and carbonation of Si-NL, leading to the formation of CSH phases (intense O–H band at $+6.2$ ppm). Negative NMR $\delta(^1\text{H})$ shifts (*) might correspond to spinning sidebands. The schematic in (d) represents the expected silica/CSH moieties present in the nanocoatings.

(Table S2, Supporting Information), a strong interaction with negatively charged deprotonated silica derivatives takes place, resulting in the formation of silica-coatings on the portlandite nanoparticles.^[36,45] This fortuitous silica functionalization of nanolimes is of special interest, as it opens up unexplored frontiers in the field of stone consolidation. For this reason, the synthesis was replicated using a Teflon reactor in the presence of pure tetraethyl orthosilicate (TEOS) to simulate the effect of the silica lixiviated from the glassware. The use of TEOS was preferred over other silicates (e.g., K_2SiO_3 or Na_2SiO_3) to avoid coprecipitation of nonportlandite solids during solvent evaporation, thus eliminating the need for further purification steps. In practice, 50 mg TEOS were added prior to the hydrolysis of calcium ethoxide, which resulted in a product (TEOS-NL) with similar characteristics as the one obtained via fortuitous silica functionalization, suggesting that controlled mass production of silica-functionalized nanolime is feasible (Figures S5–S8, Supporting Information).

These observations suggest that the silica coating was key for the obtention of $\text{Ca}(\text{OH})_2$ plate-like nanoparticles with the smallest size and highest SSA of any existing nanolimes. Indeed, Kellermeier et al.^[46] have shown that trace amounts of silica (dosed as Na_2SiO_3) enabled the stabilization of prenucleation clusters (PNC, a few nm in size) and ACC nanoparticles via the formation of a surface coating that prevented further growth and transformation into crystalline CaCO_3 . It is, therefore, reasonable to assume that a similar effect was at work in our system during the formation of $\text{Ca}(\text{OH})_2$ nanoparticles, limiting their growth and resulting in smaller size and extremely high SSA.

2.3. Colloidal Behavior of Si-NL

Optical density measurements showed high colloidal stability of all tested nanolimes when dispersed in ethanol. When water was added, Calosil nanoparticles started aggregating and settled within 450 min. Flocculation was much faster in the case of Si-NL, the particles only taking 60 min to form aggregates (Figure 4a,b). Two factors could have contributed to the sedimentation mechanism: On the one hand, the addition of water might have induced particle coarsening, leading to faster settling rates. However, this effect should be minor due to the relatively low solubility of $\text{Ca}(\text{OH})_2$. On the other hand, aggregation is strongly dependent on the electrical nature of the particle-fluid interface and changes in particle surface charge likely played an important role.^[47]

Electrokinetic analyses revealed that the ζ -potential of suspensions of nanolimes in limewater decreased from $+10.7 \pm 0.4$ to -2.1 ± 0.2 mV in the case of Calosil and Si-NL,^[18] respectively, demonstrating that the silica nanocoating modified the surface charge and made the functionalized nanolimes more susceptible to aggregation in hydro-alcoholic solutions as compared to Calosil.^[45] However, the colloidal stability of Si-NL in alcohol was not altered by the silica coating. Having the ability to induce on-demand sedimentation of nanoparticles inside a porous substrate by changing the dielectric constant (ϵ) of the carrier solvent right after applying the nanolime treatment, is an interesting result for practitioners working in the field of heritage conservation. In this way, the treatment efficacy can be maximized by preventing back-migration during solvent evaporation, which is one of the main drawbacks of this type

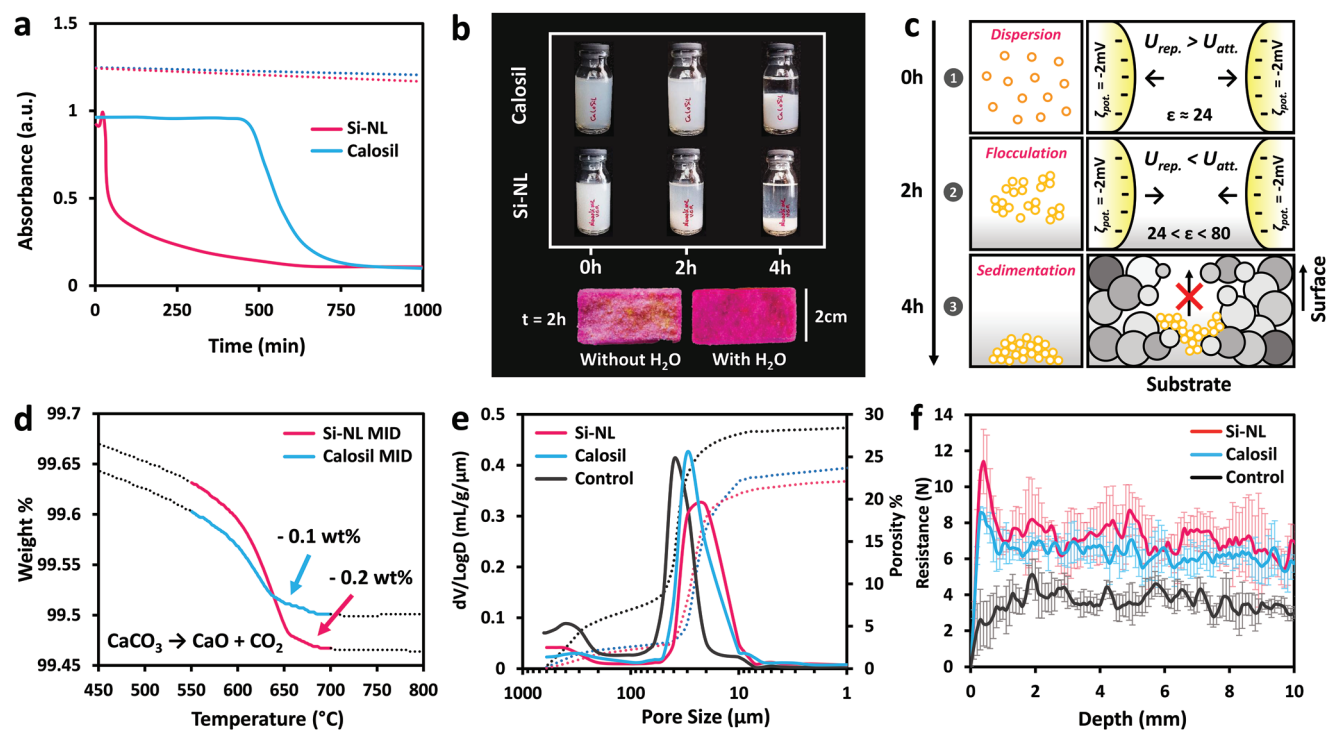


Figure 4. a,b) Colloidal behavior of Si-NL and Calosil hydro-alcoholic dispersions analyzed by optical density measurements. Dashed and solid lines in (a) correspond to dispersions in pure ethanol and ethanol–water, respectively. The phenolphthalein test (bottom images in (b)) demonstrated that the addition of water induced on-demand aggregation and inhibited back-migration, as detailed in the c) schematic. Consolidation effects of Si-NL treatments (red curves) on cured sandstone specimens as compared to Calosil treatments (blue curves) and an untreated control sample (black curve), measured by means of d) TGA, e) MIP, and f) drilling resistance, proving that silica-functionalized Si-NL distributed more homogeneously along the stone depth profile than Calosil (i.e., double the amount of decomposed CaCO_3 (TGA results) in the core of sandstone samples treated with Si-NL), originating a sharper decrease in the total porosity and median pore size, and conferring a remarkable drilling resistance over the entire drilling profile (error bars indicate the St.Dev.).

of consolidants, greatly contributing to the formation of poorly soluble CaCO_3 veils that cause dramatic color changes of the treated surface and limits in-depth consolidation (Figures S9 and S10, Supporting Information).^[48–50]

Spraying a phenolphthalein solution on freshly fractured surfaces of consolidated sandstone slabs confirmed that the application of nanolimes resulted in a homogeneous distribution of the $\text{Ca}(\text{OH})_2$ nanoparticles inside the treated sandstone specimens immediately after application. However, the material underwent significant back-migration during solvent evaporation, being accumulated in a few mm-thick surface layer after only two hours (Figure 4b-left image). This effect was substantially reduced, especially in the case of Si-NL, when water (i.e., 5 mL cm^{-2}) was applied on the stone surface minutes after the consolidation treatment (Figure 4b-right image). The beneficial effect of the water application was confirmed by TGA analyses of samples collected from the core of the treated specimens (i.e., 1 cm depth), revealing that nanolimes were distributed throughout the porous sandstone specimens. Remarkably, the measured weight loss corresponding to CaCO_3 decomposition was approximately double in the case of samples treated with Si-NL than those treated with Calosil (Figure 4d; Figure S11, Supporting Information), suggesting a more homogeneous distribution of Si-NL inside the porous system due to a more efficient aggregation after the application of water, while Calosil tended to form crusts on the treated surface.

2.4. Consolidation Tests

Mercury intrusion porosimetry (MIP) results showed a significant porosity reduction of 20.2% and 14.6% for Si-NL and Calosil treated sandstone, respectively, as compared to the untreated control (i.e., total porosity of untreated control samples and specimens treated with Si-NL and Calosil being 28.7%, 22.9%, and 24.5%, respectively) (Figure 4e). Furthermore, the median pore size decreased from $40 \mu\text{m}$ (untreated control) to 30 and $20 \mu\text{m}$ upon treatments in the case of Calosil and Si-NL, respectively, as nanoparticles deposited and carbonated within the porous system. The volume corresponding to pores with diameters larger than $100 \mu\text{m}$ also experienced a sharp reduction, consistent with the filling-in effect of the treatment.

Drilling resistance measurements provided additional proof for the effectiveness of the nanolime treatments. The drilling resistance of treated sandstone increased consistently over the whole drilling profile, by $3.51 \pm 1.17 \text{ N}$ ($101.5 \pm 33.8\%$) and $2.84 \pm 0.80 \text{ N}$ ($82.1 \pm 23.1\%$) in the case of Si-NL and Calosil, respectively (Figure 4f). The higher mechanical resistance shown by the sandstone specimens treated with Si-NL is in good agreement with the greater reduction in total porosity and the presence of silica/CSH interfaces acting as coupling agents between the newly formed CaCO_3 cement and the sandstone substrate, also enhancing the aggregation behavior of nanoparticles as previously mentioned.^[36]

Spectrophotometric results showed that the treatments affected the chromatic appearance of the stone surfaces due to the formation of a white veil, which led to an increase in luminosity (i.e., ΔL^* values being 11.8 ± 1.9 and 12.4 ± 1.6 for Si-NL and Calosil treated surfaces, respectively), being the main cause of the overall chromatic changes (i.e., ΔE^* values being 12.9 ± 1.1 and 13.3 ± 1.7 for Si-NL and Calosil, respectively). This is problematic, since conservation treatments should not produce visually detectable chromatic changes (i.e., $\Delta E > 3.0$).^[51] Here, highly concentrated nanolime dispersions of up to 25 g L^{-1} were used to obtain a maximum strengthening effect. Therefore, to avoid the formation of white veils, the use of less concentrated dispersions and immediate elimination of excess surface deposits using a wet cloth is recommended, as it is routinely done by conservators applying nanolimes in the field.^[52]

2.5. Mechanism of Carbonation and Consolidation

The comparison of the carbonation kinetics between Si-NL and the commercial Calosil nanolime revealed a much faster carbonation rate and a higher portlandite-to-calcite conversion efficacy of the former, being $\approx 86\%$ in the case of Si-NL and only $\approx 40\%$ in the case of Calosil after 72 h (Figure S4b, Supporting Information). These are very promising results, as overcoming low conversion efficacy has been one of the most challenging issues in the development of commercial products for gas capture applications.

In the particular case of heritage conservation, fast carbonation is also a highly desirable feature for nanolimes, as it also ensures a rapid consolidation effect.^[1] Remarkably, silica nanofilms did not reduce the reactivity of $\text{Ca}(\text{OH})_2$ nanoparticles. In fact, these highly porous condensed polymeric silica species seemed to have contributed to a faster carbonation rate and better consolidation efficacy by a mechanism that implies enhanced water absorption and can be summarized below.

First, at high humidity conditions (80% RH), water condensates on the surface of Si-NL and is quickly absorbed by the highly porous silica nanocoating. This initial transport of liquid water allows the dissolution of the calcium hydroxide particles, leading to a pH increase and a partial dissolution of the silica coating. Subsequently, free Ca^{2+} interacts with the silica derivatives leached from the coating to form a CSH interface (Figure 5a).^[36]

In a second stage, atmospheric CO_2 capture is promoted by the high pH at the surface of Si-NL nanoparticles ($\text{pH} \approx 12.4$), proceeding via the formation of HCO_3^- ions that readily dissociate to form H^+ that neutralize OH^- originated from the dissolution of calcium hydroxide, and CO_3^{2-} that interacts with the remaining free Ca^{2+} ions to form CaCO_3 (Figure 5b). It is not likely that the released product H_2O interferes with this process as water will diffuse out of the $\text{Ca}(\text{OH})_2$ -solution interface through the porous Si-coating, allowing both the nanoparticles and the coatings to stay almost intact during carbonation. Indeed, product H_2O probably contributes to the progress of the carbonation reaction by enabling further dissolution of portlandite (i.e., autocatalytic carbonation).^[28]

Finally, in the case of silicate substrates (sandstone in this case), the silica nanofilm acts as a self-integrated coupling

agent between the substrate and the CaCO_3 cement. New Si–O–Si covalent bonds are formed by the hydrolysis and condensation of terminal Si–OH groups from both the sandstone (i.e., from mineral phases such as quartz and feldspar)^[53] and the silica/CSH covering the nanoparticles, conferring greater mechanical strength to the consolidated substrate (Figure 5c,d) as evidenced by the drilling resistance tests. This effect solves another important drawback of conventional nanolimes when used as consolidants, as CaCO_3 by itself would not establish covalent bonds with non-calcareous substrates such as sandstone, thus only acting as pore fillers.^[54]

3. Conclusion

In this work we describe a novel and easily reproducible, high-yield solvothermal procedure for the synthesis of silica-functionalized nanolimes for their application as consolidants in the conservation and restoration of the built and archaeological heritage, involving the formation and hydrolysis of calcium ethoxide as the main intermediate species.

Based on FTIR, TEM, STEM/EDX, and solid state ^{29}Si and ^1H NMR results we demonstrate that considerable amounts of different silica-derived species (i.e., monomeric and/or polymeric), including CSH, silica-gel and siloxanes, accumulates on the surface of nanolimes in the form of a porous film that inhibited crystal growth upon adsorption on portlandite faces, thus limiting coarsening effects, irreversible oriented aggregation and allowing for a better control of the particle size. Altogether, these effects lead to the production of very small, plate-like portlandite nanoparticles, displaying surface area values nearly two times higher than those of commercial nanolimes.

Functionalization is a promising strategy to solve two of the most common handicaps of nanolimes when used as consolidants, including the control over back-migration and the lack of cohesion between the new CaCO_3 cement (i.e., from $\text{Ca}(\text{OH})_2$ carbonation) and the treated substrate, typically diminishing the efficacy of the consolidation treatment.

Significant differences in the ζ -potential and kinetic stability between limewater suspensions of Si-NL and Calosil demonstrated that silica nanofilms affected the electrostatic nature of the surface of nanoparticles and their colloidal behavior. While pure calcium hydroxide particles (Calosil) showed high stability over time, Si-NL particles aggregated much faster when dispersed in a hydroalcoholic solution. However, they both showed a remarkable stability when dispersed in ethanol, which is a key feature for the proper application of nanoparticle-based consolidant treatments. Back-migration of Si-NL nanoparticles, one of the most important drawbacks of nanolimes, was drastically reduced by simply changing the dielectric constant of the carrier solvent, inducing an effective on-demand aggregation of the particles, as shown by the phenolphthalein tests. TGA analyses of samples collected from the innermost part of the treated sandstone blocks confirmed that in the case of Si-NL, back-migration and the problematic accumulation of CaCO_3 near the surface was significantly reduced after the application of a small volume of water.

Furthermore, functionalization did not negatively interfere with the subsequent carbonation of the calcium hydroxide

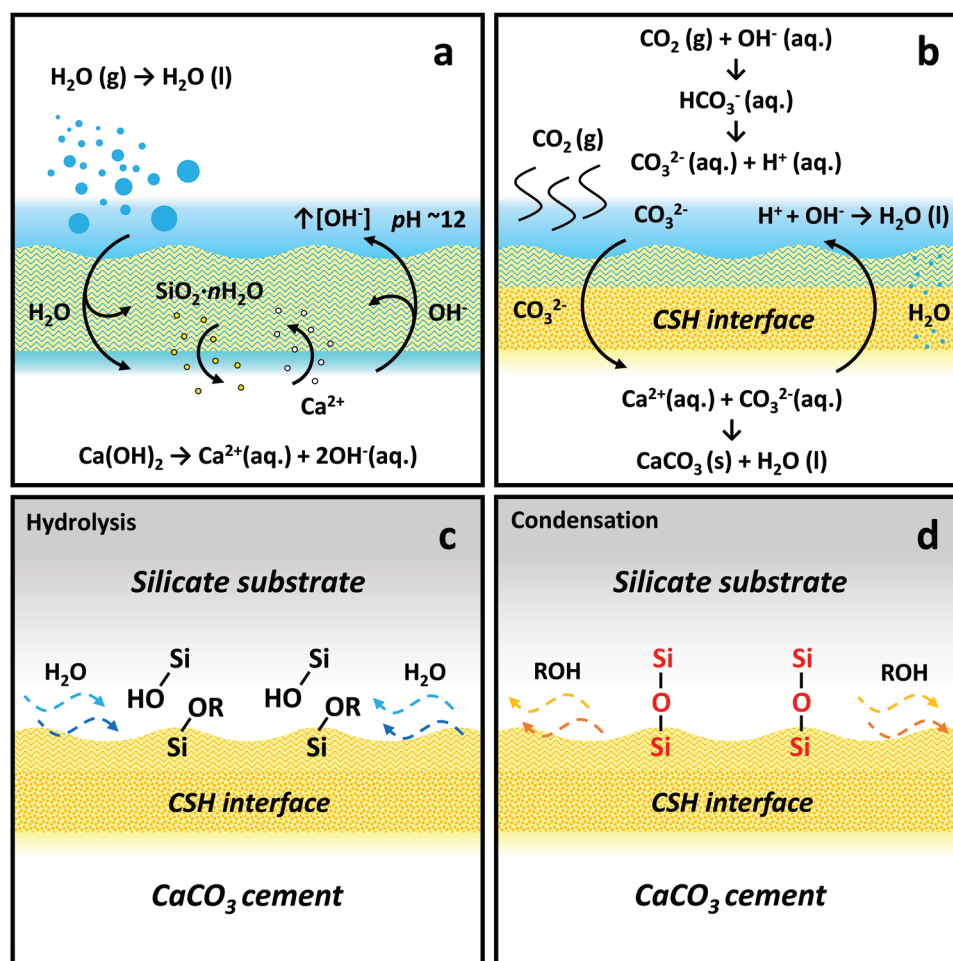


Figure 5. Schematic representation of the carbonation of Si-NL, and CSH formation. In a first stage a) water condensates on the surface of Si-NL and penetrates through the porous silica nanofilm, facilitating the dissolution of calcium hydroxide. This phenomenon gives rise to an increase in pH and the free Ca^{2+} concentration, enabling the partial dissolution of the silica nanofilm and the precipitation of CSH phases. Afterwards, b) CO_2 is hydrated to HCO_3^- , which quickly dissociates to form CO_3^{2-} that interacts with free Ca^{2+} to precipitate CaCO_3 . Coupling of the Si-NL nanoparticles to the silicate substrate occurs via c) hydrolysis and d) condensation of terminal silanol groups from both the substrate and the silica nanofilms covering the newly formed CaCO_3 cement.

particles, but was even beneficial as the highly porous silica facilitated water absorption and the partial dissolution of Ca(OH)_2 , catalyzing the capture of CO_2 in the highly alkaline pore solution, fostering and the precipitation of CaCO_3 cement. Most importantly, it enabled the formation of silica/CSH interfaces, which acted as coupling agents between the consolidant and the treated silicate substrate by establishing strong covalent Si–O–Si bonds, as shown by the increase in the drilling resistance of the stone specimens treated with Si-NL.

Finally, the fortuitous silica functionalization set the fundamentals for the synthesis of TEOS-functionalized nanolimes in non-glass reactors, displaying similar features as those obtained using glassware. The latter demonstrates the enormous potential of this methodology for controlled and scalable industrial production of functionalized nanolimes with a huge added value. The production of functionalized nanolimes could mark a major milestone for the conservation of cultural heritage, as well as for the development of advanced nanomaterials for building, environmental, or biomedical applications. For

instance, functionalized nanolimes could find high added-value applications in fields such as dentistry (e.g., root-canal endodontics) and biomedicine/biomaterials (e.g., bone-grafting).

Supporting Information

Supporting Information is available from the Wiley Online Library or from the author.

Acknowledgements

This research was funded by the MCIN/AEI/10.13039/501100011033 and the ERDF “A way of making Europe” (Spanish Government grant PID2021-125305NB-I00), the Junta de Andalucía (Research Group RNM-179 and grant P20-00675) and the University of Granada, UGR (Research Excellence Unit UCE-PP2016-05 “Carbonates”). M.B.R. was funded through a predoctoral research contract by the Spanish Ministry of Science and Innovation (Spanish Government grants

RTI2018-099565-B-I00 and PRE2019-090256), TEM, SEM, TGA, and XRF analyses were carried out at the Centro de Instrumentación Científica (CIC), UGR. The authors are very grateful to the technical personnel of University of Konstanz for performing the solid-state NMR experiments. Open access was funded by the Universidad de Granada/CBUA.

Conflict of Interest

The authors declare no conflict of interest.

Data Availability Statement

The data that support the findings of this study are available in the supplementary material of this article.

Keywords

consolidation, crystallization, mineral binders, nanolimes, nanoparticles

Received: January 20, 2023

Revised: March 25, 2023

Published online:

- [1] C. Rodríguez-Navarro, E. Ruiz-Agudo, *Pure Appl. Chem.* **2018**, *90*, 523.
- [2] C. Rodríguez-Navarro, E. Sebastian, *Sci. Total Environm.* **1996**, *187*, 79.
- [3] E. Winkler, in *Stone in Architecture: Properties, Durability*, 3rd edition, Springer, Berlin **1997**.
- [4] T. Warscheid, J. Braams, *Int. Biodeterior. Biodegrad.* **2000**, *46*, 343.
- [5] I. Jimenez-Gonzalez, C. Rodríguez-Navarro, G. W. Scherer, *J. Geophys. Res. Earth Surf.* **2008**, *113*, F02021.
- [6] E. Doehne, C. A. Price, *Stone Conservation: An Overview of Current Research*, 2nd ed., Getty Conservation Institute, Los Angeles **2010**.
- [7] M. Schiro, E. Ruiz-Agudo, C. Rodríguez-Navarro, *Phys. Rev. Lett.* **2012**, *109*, 265503.
- [8] V. Vergès-Belmin, *Illustrated Glossary on Stone Deterioration Patterns*, ICOMOS International Scientific Committee for Stone, Charenton-le-Pont **2008**.
- [9] L. Lazzarini, M. L. Tabasso, *Il Restauro della Pietra*, Cedam, Milan **1986**.
- [10] C. Selwitz, *Epoxy Resins in Stone Conservation*, Getty Publications, USA **1992**.
- [11] G. W. Scherer, G. S. Wheeler, *Key Eng. Mater.* **2009**, *391*, 1.
- [12] a) M. Baglioni, G. Poggi, D. Chelazzi, P. Baglioni, *Molecules* **2021**, *26*, 3967; b) D. Chelazzi, R. Giorgi, P. Baglioni, *Angew. Chem., Int. Ed.* **2018**, *57*, 7296.
- [13] R. Giorgi, M. Baglioni, D. Berti, P. Baglioni, *Acc. Chem. Res.* **2010**, *43*, 695.
- [14] M. Favaro, P. Tomasin, F. Ossola, P. A. Vigato, *Appl. Organomet. Chem.* **2008**, *22*, 698.
- [15] E. Hansen, E. Doehne, J. Fidler, J. Larson, B. Martin, M. Matteini, C. Rodríguez-Navarro, E. S. Pardo, C. Price, A. de Tagle, J. M. Teutonico, N. Weiss, *Stud. Conserv.* **2003**, *48*, 13.
- [16] J. Ashurst, N. Ashurst, in *Practical Building Conservation, Stone Masonry*, Vol. 1, Halsted Press, NY, USA **1988**.
- [17] R. S. Boynton, *Chemistry and Technology of Lime and Limestone*, Wiley, NY, USA **1980**.
- [18] C. Rodríguez-Navarro, A. Suzuki, E. Ruiz-Agudo, *Langmuir* **2013**, *29*, 11457.
- [19] P. Tomasin, G. Mondin, M. Zuena, N. El Habra, L. Nodari, L. M. Moretto, *Powder Technol.* **2019**, *344*, 260.
- [20] P. Baglioni, L. Dei, E. Ferroni, R. Giorgi, IT Pat., 1286868 (B1), **1998**.
- [21] P. Baglioni, L. Dei, R. Giorgi, C. V. Schettino, US Pat., 2005042380 (A1), **2005**.
- [22] P. Baglioni, L. Dei, L. Fratoni, P. L. O. Nosotro, M. Moroni, US Pat., 2005175530 (A1), **2005**.
- [23] C. Rodríguez-Navarro, E. Ruiz-Agudo, J. Harris, S. E. Wolf, *J. Struct. Biol.* **2016**, *196*, 260.
- [24] G. Ziegenbalg, DE Pat., 10327514 (B3), **2005**.
- [25] a) D. Kirchgessner, US Pat., 4786485 A, **1988**; b) R. J. Lee, C. Hsia, L. S. Fan, *AIChE J.* **1995**, *41*, 435. c) D. A. Kirchgessner, J. M. Lorrain, *Ind. Eng. Chem. Res.* **1987**, *26*, 2397.
- [26] a) M. Lorgouilloux, WIPO PCT Pat., 220775 A9, **2016**; b) S. Chini, M. Lorgouilloux, O. Nissen, O. Francoisse, European Pat., 3334690 B1, **2015**.
- [27] C. Rodríguez-Navarro, E. Ruiz-Agudo, M. Ortega-Huertas, E. Hansen, *Langmuir* **2005**, *21*, 10948.
- [28] G. Montes-Hernandez, A. Pommerol, F. Renard, P. Beck, E. Quirico, O. Brissaud, *Chem. Eng. J.* **2010**, *161*, 250.
- [29] M. Burgos-Ruiz, G. Pelayo-Punzano, E. Ruiz-Agudo, K. Elert, C. Rodríguez-Navarro, *Chem* **2021**, *57*, 7304.
- [30] D. C. Bradley, *Chem. Rev.* **1989**, *89*, 1317.
- [31] N. Y. Turova, E. P. Turevskaya, M. I. Yanovskaya, A. I. Yanovsky, V. G. Kessler, D. E. Tchekoukov, *Polyhedron* **1998**, *17*, 899.
- [32] R. C. Mehrotra, *J. Non-Cryst. Solids* **1988**, *100*, 1.
- [33] O. B. Koper, I. Lagadic, A. Volodin, K. J. Klabunde, *Chem. Mater.* **1997**, *9*, 2468.
- [34] T. I. Suratwala, M. L. Hanna, E. L. Miller, P. K. Whitman, I. M. Thomas, P. R. Erhmann, R. S. Maxwell, A. K. Burnham, *J. Non-Cryst. Solids* **2003**, *316*, 349.
- [35] D. Strachan, *Geochim. Cosmochim. Acta* **2017**, *219*, 111.
- [36] Q. Zheng, J. Jiang, G. Xu, J. Yu, L. Tang, S. Li, *Cryst. Growth Des.* **2020**, *20*, 2477.
- [37] X. Liu, X. Piao, Y. Wang, S. Zhu, *Energy Fuels* **2008**, *22*, 1313.
- [38] J. Higl, D. Hinder, C. Rathgeber, B. Ramming, M. Lindén, *Cem. Concr. Res.* **2021**, *142*, 106367.
- [39] C. Rodríguez-Navarro, I. Vettori, E. Ruiz-Agudo, *Langmuir* **2016**, *32*, 5183.
- [40] B. Walkley, J. L. Provis, *Mater. Today Adv.* **2019**, *1*, 100007.
- [41] E. Pustovgar, R. P. Sangodkar, A. S. Andreev, M. Palacios, B. F. Chmelka, R. J. Flatt, J. B. d'Espinosa de Lacaillerie, *Nat. Commun.* **2016**, *7*, 10952.
- [42] S. L. Brock, in *Nanoscale Materials in Chemistry*, 2nd ed. (Eds: K. J. Klabunde, R. M. Richards), John Wiley and Sons, USA **2009**, Ch. 8.
- [43] F. Rubio, J. Rubio, J. L. Oteo, *J. Sol-Gel Sci. Technol.* **1997**, *8*, 159.
- [44] F. K. Crundwell, *ACS Omega* **2017**, *2*, 1116.
- [45] C. Rodríguez-Navarro, E. Ruiz-Agudo, A. Burgos-Cara, K. Elert, E. F. Hansen, *Langmuir* **2017**, *33*, 10936.
- [46] a) M. Kellermeier, E. Melero-García, F. Glaab, R. Klein, M. Drechsler, R. Rachel, J. M. García-Ruiz, W. Kunz, *J. Am. Chem. Soc.* **2010**, *132*, 17859; b) M. Kellermeier, D. Gebauer, E. Melero-García, M. Drechsler, Y. Talmon, L. Kienle, H. Cölfen, J. M. García-Ruiz, W. Kunz, *Adv. Funct. Mater.* **2012**, *22*, 4301.
- [47] J. D. Clogston, A. K. Patri, in *Characterization of Nanoparticles Intended for Drug Delivery* (Ed: S. McNeil), Humana Press, USA **2010**, p. 63.
- [48] T. Lopez-Martinez, J. Otero, *Coatings* **2021**, *11*, 1083.
- [49] L. Normand, S. Duchêne, V. Vergès-Belmin, C. Dandrel, D. Giovannacci, W. Nowik, *Int. J.* **2020**, *14*, 1120.
- [50] G. Borsoi, B. Lubelli, R. Van Hees, R. Veiga, A. Santos Silva, *Constr. Build. Mater.* **2017**, *142*, 385.

- [51] J. Schanda, in *Colorimetry: Understanding the CIE System*, John Wiley and Sons, USA **2007**.
- [52] J. Otero, J. S. Pozo-Antonio, C. Montojo, *Mater. Struct.* **2021**, *54*, 41.
- [53] J. G. Matison, in *Silicon Surface Science* (Eds: M. Owen, P. Dvornic), Vol. 4, Springer, Dordrecht **2012**, Ch. 10.
- [54] G. Wheeler, *Alkoxysilanes and the Consolidation of Stone*, Getty Publications, USA **2005**.